Proceedings of ASME Turbo Expo 2021
Turbomachinery Technical Conference and Exposition
GT2021
June 7-11, 2021, Virtual, Online

GT2021-58941

COMPOSITE UHBR FAN FOR FORCED RESPONSE AND FLUTTER INVESTIGATIONS

Torben Eggers
Jens Friedrichs
Institute of Jet Propulsion and Turbomachinery
Technische Universität Braunschweig
38108 Braunschweig
Germany
Email: t.eggers@ifas.tu-braunschweig.de

Jan Goessling*
Joerg R. Seume
Institute of Turbomachinery and Fluid Dynamics
Leibniz Universität Hannover
Garbsen, 30823
Germany
Email: goessling@tfd.uni-hannover.de

Nunzio Natale

DREAM INNOVATION Srl
Sant'Arpino, 81030
Italy
Email: nunzio.natale@dreaminnovation.it

Jan Peter Flüh
Nicola Paletta
IBK Innovation GmbH & Co. KG
Hamburg, 21129
Germany
Email: nicola.paletta@ibk-innovation.de

ABSTRACT

In the CA3ViAR (Composite fan Aerodynamic, Aeroelastic, and Aeroacoustic Validation Rig) project, a composite low-transonic fan is designed and tested. The aim is a scaled ultra-high bypass ratio (UHBR) fan with state-of-the-art aerodynamic performance and composite rotor blades, which features aeroelastic phenomena, e.g. forced response by inlet distortions and flutter, under certain operating points within the wind tunnel. In this paper, the aerodynamic and aeroelastic design process starting from the overall performance specifications to a three-dimensional numerical model is described. A target of eigenfrequency and twist-to-plunge ratio is specified such that flutter occurs at desired operating conditions with a sufficient margin with respect to the working line. Different materials and layups of the composite blade are analyzed to reach the structural target. The fan should serve as an open test case to advance the future research on aerodynamic, aeroelastic, and aeroacoustic performance investigations in a wide range of operating conditions. A preliminary fan stage design is presented in this paper.

NOMENCLATURE

Symbols

b	blade camber
c	blade chord length
c_p	specific heat capacity
E_{mod}	modal energy
f	blade eigenfrequency
I	turbulence intensity
k	reduced frequency
l	turbulence length scale
$\dot{m}$	mass flow
Ma	Mach number
n	rotational speed
p	static pressure
p_t	total pressure
r	radius

*Address all correspondence to this author.

t	blade thickness
t_1, t_2	leading, trailing edge thickness
T_t	total temperature
u	flow velocity relative the blade
V	velocity
W_{cyc}	modal work per cycle
x_b	maximum camber position
x_t	maximum thickness position
X_{LE}	modal deformation of blade leading edge
X_{TE}	modal deformation of blade trailing edge
α	twist-to-plunge ratio
β, $\beta^{'}$	velocity flow angle
δ	logarithmic decrement
η_{poly}	polytropic efficiency
π_t	total pressure ratio
ϕ	flow coefficient
ψ	work coefficient
ν	hub-to-tip ratio
Subscripts	
$0, 1, 2, 3$	streamwise position
i	radial position
z	axial
Θ	circumferential

AIP	aerodynamic interface plane
BPR	bypass ratio
CFPR	carbon fiber reinforced polymers
DLR	German Aerospace Center
DP	design point
EO	engine order
GTF	geared turbofan
HB	Harmonic Balance
IBPA	interblade phase angle
LTF	low-transonic fan
MPC	multi-point-constraint
ND	nodal diameter
OGV	outlet guide vane
PTF	Propulsion Test Facility
SM	stall margin
TET	turbine entry temperature
UHBR	ultra-high bypass ratio
WL	working line

INTRODUCTION

In order to combine already efficient modern axial turbines with low-speed fans, the so-called geared turbofan (GTF) design allows for the decoupled development of turbine and fan; it is therefore a crucial basis for increasing the bypass ratios (BPRs). An increase in the propulsive efficiency is achieved through a lower nozzle exit velocity, along with an increased total engine mass flow with a lower fan pressure ratio. This implies larger fan diameters and thus higher bypass ratios. Such new propulsors do come with significant challenges from an aerodynamic and structural perspective. For higher engine BPR at constant nozzle design, the take-off and approach operating points of the fan move closer to the part-power limit, hence reducing its stall margin and increasing the risk of fan flutter. Flutter is a self-excited aeroelastic instability, where the interaction of blade vibration and unsteady aerodynamic forces leads to an energy transfer from the flow into the blade motion. This unsteadiness is caused by the blade vibration itself and is non-synchronous with the engine order (EO). In turbomachinery, flutter is mostly observed for the 1st flap (1F) mode, vibrating with the 1st to 6th forward traveling nodal diameter (ND). Stall flutter can occur at part-speed operating conditions close to the stall boundary and is therefore of great interest during the design of ultra-high bypass ratio (UHBR) fans. Mechanisms of stall flutter in a modern turbofan have been investigated in several studies, e.g. [1], [2]. The studies show that the stall flutter of the investigated fan blade is driven by a separated flow region on the suction surface. Another condition for flutter instability was found in the acoustic pressure field associated with the blade vibration, which must be cut-on upstream and cut-off downstream of the rotor.

In parallel, the increased fan diameter is driving the intake design. In order to reduce the wetted intake surface and its drag, intakes have to be reduced in axial length and lip thickness, which in turn increases the inlet distortion at the aerodynamic interface plane (AIP) during off-design and crosswind conditions. These inlet distortions are causing forced responses of the rotor blade at low EO. Since the forcing of the blade due to crosswind contains multiple harmonics, several EOs can be excited. High crosswind excitations can also induce significant off-resonant vibrations [3]. The intake is an important parameter for the flutter stability of the fan, whose influence increases due to the stronger coupling of rotor and shortened intake. A numerical study on aeroelastic instability for a low-speed fan proves that the fan intake reflections play a decisive role in the flutter behavior of the blade, generating the so-called flutter bite [4], which must be considered during the design process of the blade and the intake [5].

Overall, the phenomena at off-design have not yet been explained in detail and state-of-the-art methods are still unable to predict them reliably [6]. Additionally, the operating range is mostly determined by multi-physical effects, emphasizing the need for models representative of real engines in numerical simulations and experiments [7]. It is of great interest to set up a representative test case of interdisciplinary research, e.g. Brandstetter et al. [8].

Besides these increased aerodynamic requirements, the fan itself has to be reduced in weight, leading to the use of lighter and stiffer materials, such as carbon fiber reinforced polymers (CFPR) instead of more conventional titanium alloys. These provide more degrees of freedom in the design in terms of cus-

tomized stiffness and inertia distributions along the blade span, as the current trend is to improve the propulsive part of direct drive turbofans [9]. The application of CFPRs to engine fans poses new challenges regarding design and manufacture, this material being non-homogeneous and in principle anisotropic [10]. In [11] the vibration characteristics of composite fan blades are investigated, showing that a change of the composite system as well as different materials have a significant impact. It was shown that the fiber orientation has a huge influence on the deformation behavior [12]. The general need to conceive distortion-tolerant fan designs leads to the necessity of developing and validating high-fidelity numerical methods for blade loads and unsteady elastic displacements predictions. Indeed, as an increase of the fan diameter leads to slender and highly loaded blade structures, being able to accurately predict the aeroelastic and aeroacoustic behavior becomes crucial for achieving the right effectiveness of the new fan design. Furthermore, for the validation of new numerical methods at the intake-to-fan interface, an extensive test campaign on a representative test case is considered by the authors.

CA3ViAR is contributing to the achievement of Clean Sky 2 goals by designing and testing a highly instrumented composite low-transonic fan (LTF). This fan is conceived to experience forced response and instabilities, such as stall and flutter, inside a specific propulsion wind tunnel, the Propulsion Test Facility (PTF) of the Institute of Jet Propulsion and Turbomachinery. This wind tunnel provides conditions similar to real fan flows in order to investigate instabilities systematically in a lab environment [13]. The present study aims at designing a fan stage for coupled aerodynamic, aeroelastic, and aeroacoustic investigations for a representative UHBR fan stage model. Therefore, the design approach and preliminary results are presented, which will be used for the ongoing research project.

FAN STAGE DESIGN

As an interdisciplinary topic, the fan stage design requires consideration of aerodynamics, aeroelasticity, and aeroacoustics. Overall, the fan stage design is an iterative process between these disciplines, of which the preliminary results are presented here. As shown in Figure 1, the iterative design process consists of an aerodynamic and an aeroelastic tool chain. The outcome of the aerodynamic design, i.e. the geometry and the flow data, serves as input for the aeroelastic design and analysis. Despite the internal iterative loops, the tool chains are linked. For instance, if the structural design for a flutter-prone fan is not readily possible, the appropriate blade parameters can be adjusted without running the meridional design. The respective design processes are described in this chapter.

TABLE 1. FAN DESIGN PARAMETERS

	DP@10.7 km	Rig@0 km	
Operating point	Cruise	Cruise	Take-Off
Bypass ratio	17	17	17
Mach number Ma_z	0.62	0.62	0.52
Poly. efficiency η_{poly}	0.89	0.89	0.87
Total pressure ratio π_t	1.37	1.37	1.32
Mass flow $\dot{m}$ / (kg/s)	272.24	63.39	57.15
Rot. speed n / RPM	2375	8667	8095
Fan tip speed V_Θ / (m/s)	272	295	275
Fan tip radius r_{tip} / m	1.093	0.325	0.325
Hub-to-tip ratio ν	0.26	0.26	0.26

Aerodynamic design

Within the aerodynamic design process shown in Fig. 1, the dimensions and characteristics of the fan stage, as well as the shape of the blades are defined. Beginning with an engine cycle design using the performance design tool *GasTurb* [14], the key parameters of the fan stage are specified. *GasTurb* provides several engine cycles and in particular characteristic curves for each engine module depending on ambient conditions, engine mass flow, BPR, turbine entry temperature (TET) and component efficiencies. The choice of parameters is based on orders of magnitude of current engine designs [15]. The design is set for high polytropic efficiency at cruise condition, to provide an ideal open test case publication. But since most of the planned measurements and simulations will be conducted at take-off condition, this operating point will be checked during the whole design process. This applies in particular to the operating points which are of interest for the aeroelastic flutter tests. The fan is designed for a geared turbofan engine based on state-of-the-art aircraft concepts operating at a cruising altitude of 10,700 m with a flight Mach number of $Ma_{flight} = 0.78$. The take-off condition resembles an operation at $Ma_{flight} = 0$, which is the most critical flow state for cross wind investigations. This leads to a chosen bypass ratio of 17 with a fan total pressure ratio of 1.37 at a mass flow of 272 kg/s. Further design parameters are shown in Tab. 1. This performance design is in accordance to the fan stage design by Kaplan, which provides a comprehensive reference for UHBR fan stages [16]. In order to ensure the operation of the fan under test rig conditions, a theoretical working line at sea level is calculated in advance. The modular fan re-

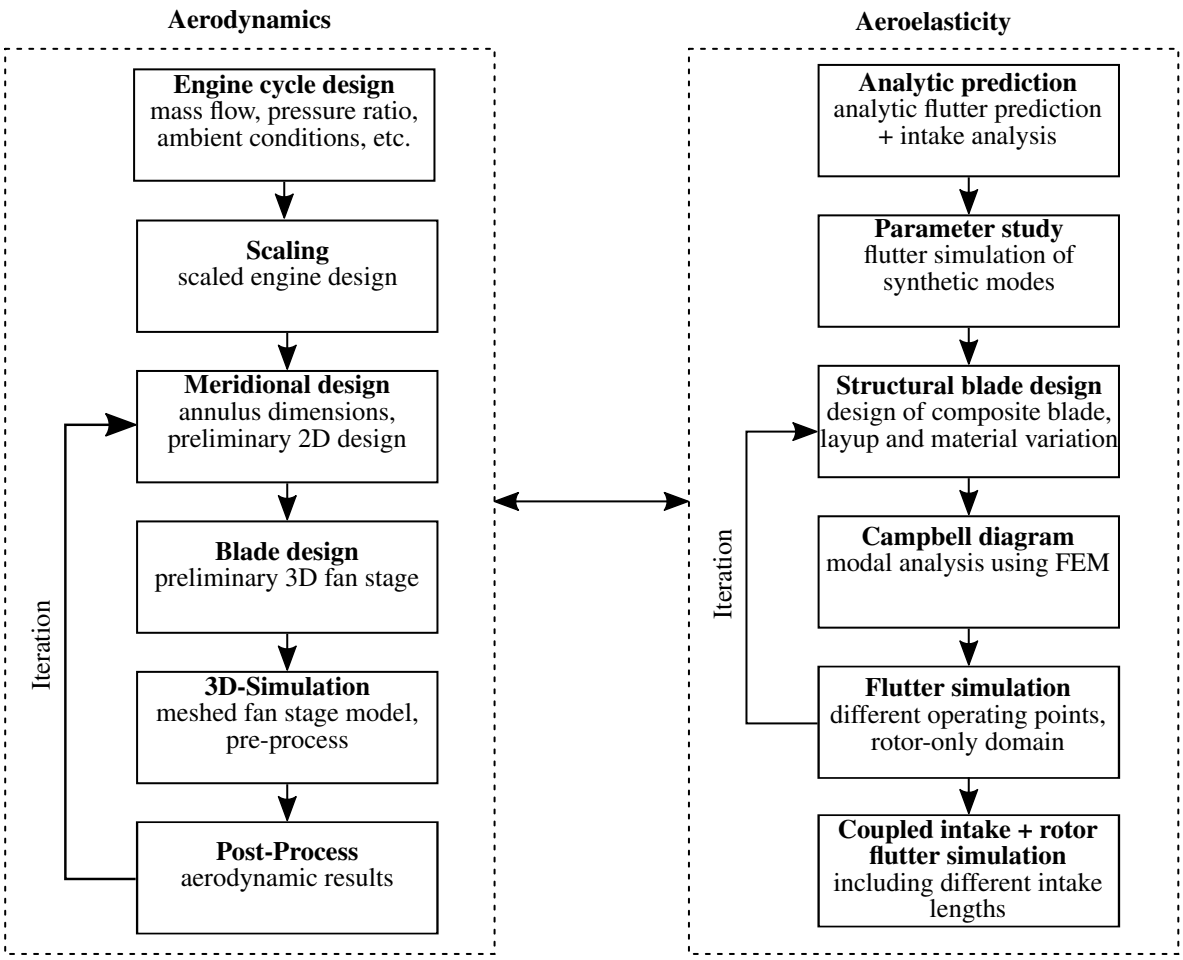

FIGURE 1. DESIGN PROCESS

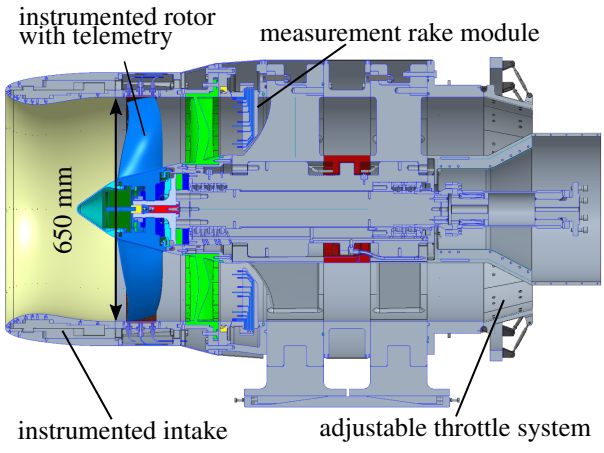

FIGURE 2. PRELIMINARY FAN RIG OF INFRa

search rig setup of a preceding project called INFRa (Integrated Nacelle Fan Rig assembly), shown in Fig. 2, serves as a foundation for the fan stage design in CA3ViAR. Following the design process in Fig. 1, the resulting thermodynamically based dimensions of a full-sized engine are scaled to the final rig dimensions. Thereby, geometrical and Mach similarity will be ensured. The resulting fan is in the scale of approximately 1:3.3 based on the *GasTurb* design. The scaled engine design serves as an input for the IFAS in-house fan stage design code, described in [17]. Based on required mass flow, pressure ratio and ambient conditions, the through-flow code iteratively computes the streamlines for both rotor and stator. Some assumptions are made in advance for the design such as negligible blade forces, steady axial symmetric flow, no local shearing effects of viscosity and no heat transfer. The code uses the isentropic radial equilibrium equation by assuming swirl-free velocities at inlet and outlet of the stage,

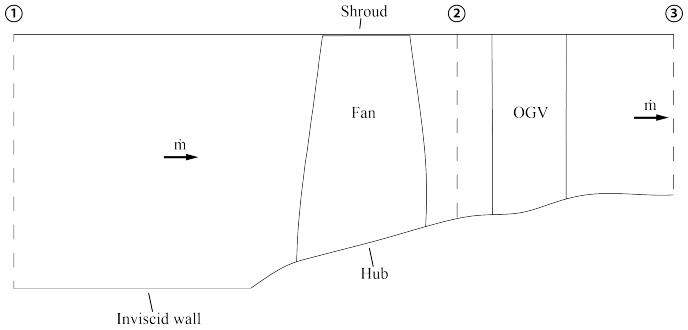

FIGURE 3. MERIDIONAL VIEW OF THE SCALED FAN STAGE

controlling the local outlet swirl and neglecting radial flow [18]. It is defined as follows:

$$V_z - V_{z,i} = 2c_p(T - T_i) - (V_\Theta^2 - V_{\Theta_i}^2) - \int_{r_i}^{r} \frac{2V_\Theta^2}{r}\mathrm{d}r \qquad (1)$$

Additional empirical correlations according to Lieblein and Carter consider flow losses and under turning effects [19]. The implementation of aerodynamic load indicators such as the diffusion factor and de Haller coefficient for efficient design control leads to a preliminary 2D design of the meridional dimensions and the corresponding radial flow distribution. The resulting 2D design of the scaled fan stage is shown in Fig. 3.

The rotor of the fan stage is referred to as fan, while the stator is named outlet guide vane (OGV). As stated before, the hub and shroud contour are defined by the geometrical constraints imposed by the choice to use the INFRa rig. For the radial load distribution, the vortex theory, published in NASA-SP-36 [18] is used. The assumption of a constant axial velocity over the stator passage leads to the radial rise of hub contour in the stator. In total, the fan stage consists of 18 rotor blades and 40 stator vanes. The rotor blade number is calculated based on the airfoil aspect ratio, which is estimated based on given trends in the literature [15], whereas the stator blade number is determined by the cut-off condition of the chosen rotor blade number to achieve the lowest possible tonal fan noise [15]. At design point (DP), the fan stage is operated with a flow coefficient of $\phi = 0.69$ and a work coefficient of $\psi = 1.59$ at a polytropic efficiency of $\eta_{poly} = 0.89$. Blade design is done for each streamline by a parabolic arc [20], superimposed with a cubic thickness distribution [21] applying the method by Abbott and von Doenhoff [22] (see Fig. 4). The equations used are described in Appendix A. An ellipse with a 3:1 ratio is used for the leading and trailing edge of the blades. With defined values for maximum camber position x_b, maximum thickness position x_t, thickness-to-chord ratio t/c, thickness at leading edge t_1 and trailing edge t_2 as well as the calculated flow parameters from the meridional design, a blade is generated by 101 radial airfoil sections. To attain the required mass flow, the

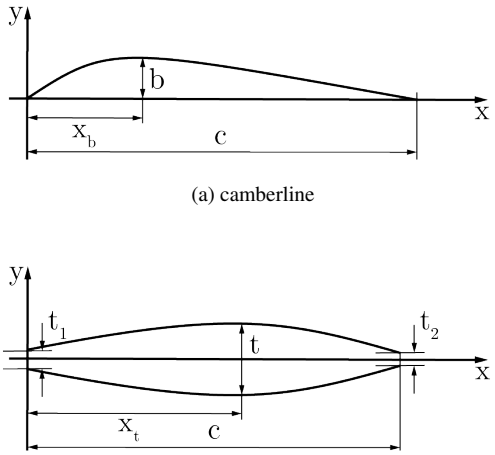

FIGURE 4. AIRFOIL PARAMETERS

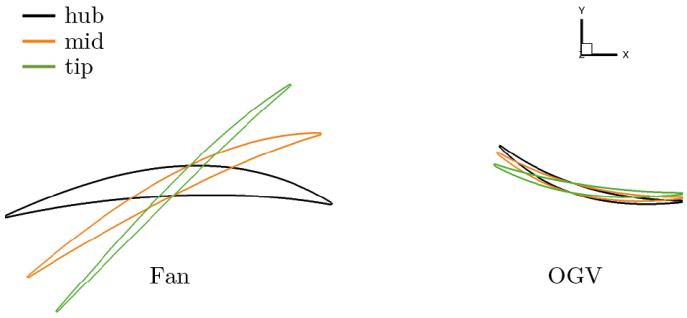

FIGURE 5. AIRFOIL SECTIONS OF THE FAN STAGE

transonic rotor sections are staggered with regards to the unique incidence conditions to match the inflow conditions and the airfoil geometry. By radial staggering the airfoils in the center of gravity, the preliminary 3D fan stage is created. The running tip clearance is chosen to be 0.5 *mm*. Figure 5 shows the staggered airfoil sections of the fan and the OGV at hub, mid and tip radius. The meridional and blade design are directly connected to the aeroelastic and aeroacoustic design, as any changes to the fan stage are adopted in those process steps. The blade design is subject to further requirements. Due to the ply layup, the minimum thickness of the blade may not be less than 0.62 mm to ensure manufacturability.

Aeroelastic design process

The aim of the aeroelastic design is to achieve a composite rotor blade, which generates aeroelastic phenomena within the operating range of the rig. These aeroelastic phenomena are

forced response, where the blade is excited by the inlet distortions induced by the crosswind tunnel of the PTF, and flutter, which is a self-exciting phenomenon. For forced response, the Campbell diagram of the composite blade is simulated and crossings of the blade eigenfrequencies with the EOs define the operating points at which forced response occurs. To excite the rotor of the fan using crosswind, an eigenfrequency of the fan blade must cross a low EO within the possible rotational speeds of the rig. The distortion of the crosswind contains multiple harmonics, which result in the forcing of the rotor with several nodal diameters. At high crosswind amplitudes, there can be a significant off-resonant response of the blade vibration [3]. Based on the literature, EOs up to 8 are considered for possible excitation by inlet distortions, e.g. [23].

Operating points of a LTF prone to flutter are in general more difficult to predict and to control than forced response. During the aeroelastic design process, the focus is on the stall flutter of the rotor blades. The composite blade material and layup in the fan rig is designed such that (1) stall flutter occurs at low mass flow rates off the working line while (2) sufficient margin in aerodynamic damping exist on the working line. The steps of the aeroelastic design process are summarized in Fig. 1. First, the reduced frequency is used to analyze different operating points and blade frequencies. The reduced frequency is defined by

$$k = 2\pi \frac{fc}{u}, \tag{2}$$

including the blade frequency f, the chord length c and the flow velocity relative to the blade u. Further analytic predictions of nodal diameters and rotational speeds at which flutter might occur are based on the cut-on condition of acoustic modes propagating up- and downstream of the rotor. The acoustic mode upstream must be cut-on and the mode propagating downstream of the rotor must be cut-off for flutter condition. Also, the influence of the intake reflection on the blade stability of the fan is analyzed analytically by using a similar approach to the method described in [24]. A parameter study is performed by simulating flutter with a preliminary aerodynamic design with varying mode shapes and eigenfrequencies to understand the flutter behavior of the scaled fan and to define a first target for the design of the composite layup and material. The target includes the blade eigenfrequency and the twist-to-plunge ratio. The twist-to-plunge ratio is the ratio of the mode shape's deformation twist angle amplitude to the plunge amplitude times the semi-chord of the blade. The ratio is calculated as

$$\alpha = \frac{2\,(X_{LE} - X_{TE})}{X_{LE} + X_{TE}}, \tag{3}$$

where X_{LE} is the deformation at the leading edge and X_{TE} is the deformation at the trailing edge of the mode shape. Based on the target parameters, different structural blade designs with varying materials and layups are generated and their eigenfrequencies and mode shapes are calculated with FEM software. By including the rotational effects, the Campbell diagram is calculated. Each blade design is checked to ensure the safety margins. The resulting mode shapes and eigenfrequencies are used for the 3D-flutter simulations of the rotor blade at several operating conditions. Depending on the outcome of the rotor-only flutter simulations, a new composite blade is designed.

If a promising structural blade design is found during the iterative process within the rotor-only domain, the coupled simulation of the intake and the rotor are performed. This allows quantifying the effect of the intake on the aerodynamic damping. Different intake lengths will be analyzed at different rotational speeds, mass flows, and interblade phase angle (IBPA).

NUMERICAL SETUP

Numerical Setup of Aerodynamics

To achieve high-fidelity CFD results, a high-resolution mesh with low-Reynolds configurations is set up. Based on the airfoil sections a volume model is created within *NUMECA AutoGrid5* to mesh the fan stage. For preliminary fan design the dimensionless wall distance was chosen to be $y^+ = 1$ at the blade, hub and shroud walls. The required mesh density was determined using the grid convergence index (GCI) to ensure mesh independent results [25]. With a maximum GCI of about 0.01% for the mass flow the results can be stated as mesh independent. The mesh size for the fan stage is about 4.1×10^6 cells with 137 cells in radial direction in a single pitch periodic domain. The Pre-Process for the simulations in *TRACE* is done with *GMC 9.1.7*, defining the solver settings and boundary conditions for the 3D fan stage model. To decrease the design process time, the pre-process including mesh generation is built up in a semi-automatic way. Simulations are conducted at steady state conditions for the hot blade geometry. The two equation k-ω turbulence model with modifications of the turbulence production near stagnation points and in areas with high streamline curvature is chosen since it is able to provide good and reliable results for reasonable computational costs. Within *TRACE*, these modifications are the stagnation point anomaly fix by Kato and Launder [26], rotational effects by Bardina [27], and compressibility effects [28]. In order to incorporate the important effect of laminar-turbulent boundary layer transition in LTFs, the k-ω model will be used in conjunction with the γ-$Re\Theta$ two-equation transition model [29]. The interface between the rotating fan domain and the stationary OGV domain is modeled with a mixing plane approach. For the preliminary design, the rotor-stator interaction will not be investigated. The hub is defined as a non-viscous wall in the inlet area, because the hub contour is not modeled down to the machine axis (Fig. 3). The radial inlet boundary profile is defined by homogeneous ambient conditions at sea level, assuming a total-pressure

TABLE 2. NUMERICAL SETTINGS

	Parameter	
Setting	Aerodynamics	Flutter
Mode	RANS	HB
Wall treatment	Low-Reynolds	Low-Reynolds
Inlet	$p_{t,1}$, $T_{t,1}$, β_1, β'_1, l, I, Ma	
Outlet	p_3	p_2
Interface	Mixing plane	-
Turbulence model	k-ω	k-ω
Transition model	γ-$Re\Theta$	γ-$Re\Theta$
No. of Harmonics	-	1

loss of 1% due to nacelle diffusion. Additionally, an axial flow with a low turbulence intensity of 1% is applied. The outlet is defined by a static pressure at midspan. The final numerical settings at design point operation are summarized in Tab. 2. For off-design simulations, the rotational speed and the static pressure are adjusted accordingly. It is worth specifying that no geometrical changes due to centrifugal forces are taken into account in the preliminary aerodynamic design process. This aspect will be checked after the completion of the structural design of the test article and a sufficient margin will be added for safety.

Numerical Setup of Aeroelastic

The aeroelastic analysis consists of two parts: the modal analysis and the flutter analysis. The modal analysis provides the input for the Campbell diagram to validate the plausibility of the blade design by checking the compliance with the NASA requirements CR-174992 [30] and it provides the nodal displacements of the eigenmodes for the flutter analysis.
The flutter analysis characterizes the aerodynamic damping behavior of the rotor blade for specific operating points.

Modal Analysis The modal analysis is performed using the Lanczos method from *Nastran* solution 103. This is the default setup for performing a modal analysis with *Nastran* and offers the best results for most problems. To identify the best suitable blade design for the needs of the CA3ViAR project, the modal analysis must be performed numerous times using different materials, layups and rotational speeds. Therefore, the complexity of the model should not be higher than necessary to provide a short calculation time. The FE model for the analysis is created with *Patran 2012.2.2* using shell elements with the respective composite properties. The convergence study shows that 5k elements (Fig. 6) are sufficient for the modal analysis. Doubling the element amount leads to a change in the results of less than 0.1%. The color plot in Fig. 6 shows the thickness distribution of the blade in mm and the orientation of the different layers. The composite blades are physically clamped at the root by means of suitable metallic parts (frame and wedge). The entire root is inserted and clamped. The root part of the model is constrained with a rigid RBE2 multi-point-constraint (MPC), which prevents the movement of the nodes and provides the stiffness needed to simulate the clamping of the blades at the hub. These fixed constraints have been verified by past experiences using the same design of the joint. Moreover, this connection is used to introduce the rotational forces into the model. Fig. 6 also shows the application of aerodynamic loads for the stress and fatigue analysis for which load results from the aerodynamic analysis are extracted. Following the stripe wise extraction, the loads are applied to the quarter chord of the blade model at the points 1-10 and are distributed over the stripes using RBE3 MPC. The stress and fatigue analyses are not part of this paper. Therefore, it is only mentioned here that both are not critical for the presented blade design.

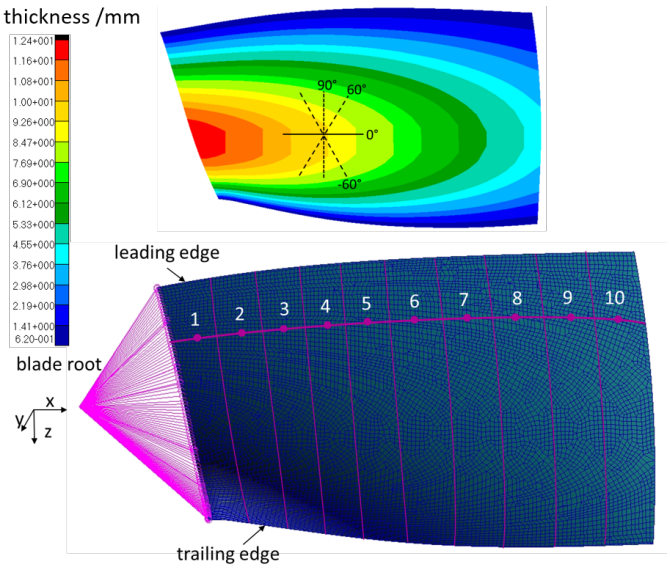

FIGURE 6. MODEL FOR MODAL ANALYSIS

Flutter Simulation The flutter simulations of the rotor-only domain and the coupled domain, including the intake and rotor are performed with the nonlinear research solver *TRACE* Harmonic Balance (HB) developed by the German Aerospace Center (DLR). The solver computes the unsteady RANS equations in the frequency domain, assuming that the unsteady part can be represented by Fourier series. The solver and the method

used is described in detail in [31]. Based on the steady-state solution of the 3D-simulation within the aerodynamic design, an unidirectional flutter simulation is performed. Within the flutter simulation, the blade is vibrating with a constant mode shape and amplitude, inducing the unsteady flow field, e.g. the unsteady pressure distribution on the blade surface. The mode shape is mapped with a max. amplitude of 0.1 mm, which deforms the CFD mesh. The logarithmic decrement δ is used to describe the resulting aerodynamic damping and is calculated by

$$\delta = -\frac{\Re(W_{cyc})}{2E_{mod}}. \tag{4}$$

The modal work per cycle $\Re(W_{cyc})$ is calculated from the unsteady pressure field on the blade surface and the blade velocity. The modal energy E_{mod} is calculated with the deformation of the blade, the vibrational frequency, and the modal mass of the mode shape. The calculation and mapping procedure are explained in [32]. For the flutter simulation of the rotor-only setup, the rotor mesh domain of the aerodynamic design is used and the numerical settings are shown in Tab. 2. The same transition model and turbulence model settings are used as in the aerodynamic design. This allows a direct restart of the unsteady flutter simulation in the frequency domain based on the simulation results of the aerodynamic design. The unsteady turbulence and transition effects are included. The mean flow (0th harmonic) and the 1st harmonic of the blade vibration frequency is resolved in the simulation. The influence of higher harmonics on the aerodynamic damping has been analyzed during preliminary studies and considered to be small enough to use only one harmonic during the design process to decrease the required computation time.

RESULTS

Several iterations were performed to fulfill the design criteria given in Tab. 1. The design procedure is still ongoing, of which the current results are shown in this paper. The 3D CFD results are analyzed and compared with the prescribed design values. Adjustments to the meridional or blade design are made iteratively to fulfill the design requirements. Thereby, the blade design is adjusted to account for the actual incidence angles. The camber of the transonic flow blade sections was reduced iteratively to change the shock pattern on the fan suction side by controlling the throat area parameter of the fan passage. The blade geometry matching the aerodynamic and aeroelastic specifications is shown in Fig. 7, outlining the numerical domain.
Within the aeroelastic design process, operating points prone to flutter have been identified with analytic prediction methods. By varying the eigenfrequency and the mode shape in the flutter

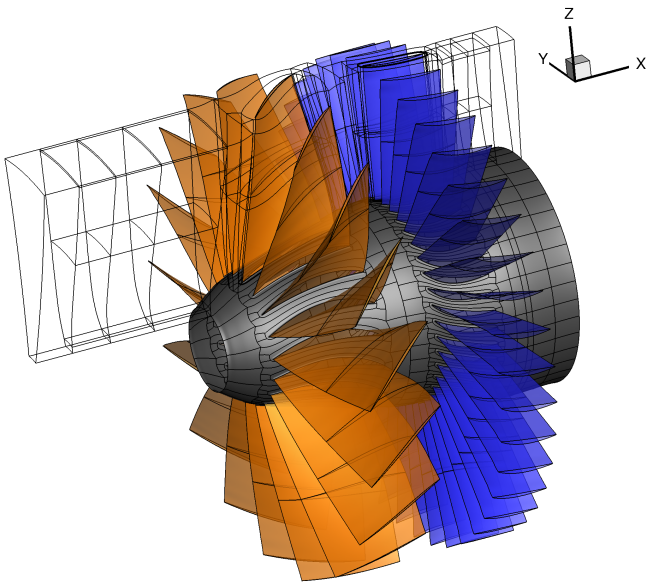

FIGURE 7. FAN STAGE MODEL

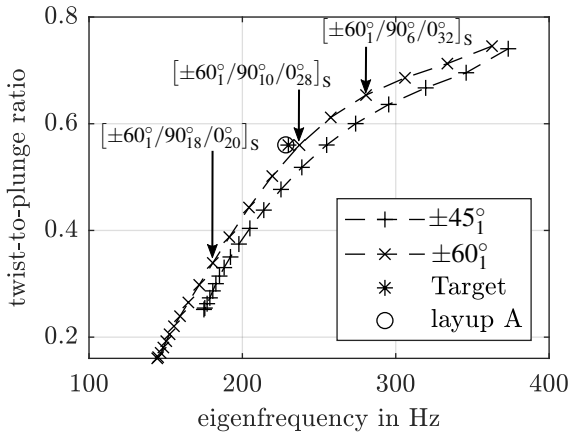

FIGURE 8. EIGENFREQUENCY AND TWIST-TO-PLUNGE RATIO OF DIFFERENT LAYUPS USING T300 MATERIAL AT 7500 RPM

simulations during the parameter study, a target of an eigenfrequency of 230 Hz and a twist-to-plunge ratio of 0.56 is defined. The reduced frequency at 7500 RPM on the working line is approx. $k = 0.7$ at 90% radial channel height. During the iterative design process with different composite blade designs, those designs close to these values provided unstable conditions at low mass flow rates off the working line, as required above. Additionally, these designs also achieved stable conditions with a good margin in aerodynamic damping on the working line, thereby fulfilling both of the requirements above. Dif-

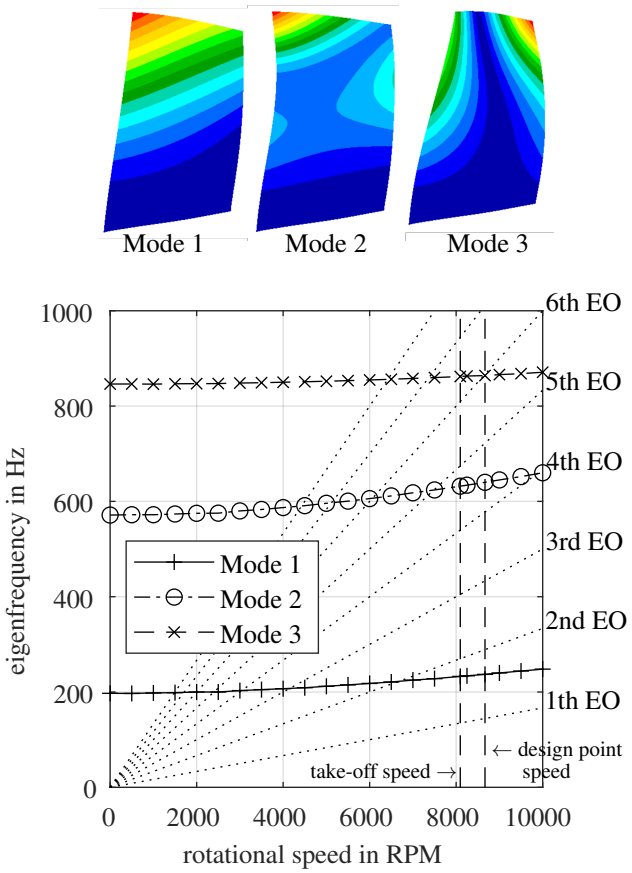

FIGURE 9. CAMPBELL DIAGRAM OF LAYUP A

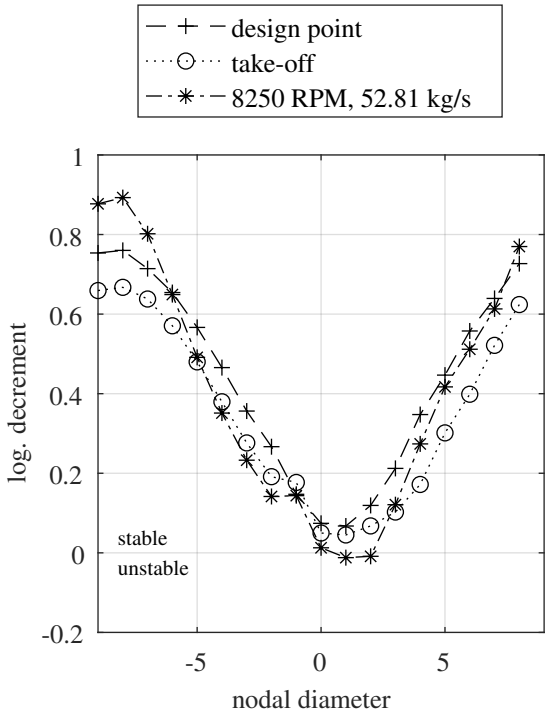

FIGURE 10. AERODYNAMIC DAMPING OF EACH NODAL DIAMETER AT KEY OPERATING POINTS, MODE 1

ferent materials and layups are tested to fulfill the set requirements. Figure 8 shows the resulting eigenfrequency and twist-to-plunge ratio of blade layups with $1 \pm 45°$ and $1 \pm 60°$ target layer with increasing 90° plies within the blade. By increasing the number of 90° plies, the bending stiffness and thereby the eigenfrequency can be lowered. However, decreasing the bending stiffness of the blade while keeping the torsional stiffness at the same level also decreases the twist-to-plunge ratio, which is dependent on the ratio of bending stiffness and torsional stiffness. Therefore, the solution with ±60° layers on the outside instead of the typical design with ±45° outside layers seems more promising for achieving the target with the current blade geometry. With an eigenfrequency of 228 Hz and a twist-to-plunge ratio of 0.56, the layup A with a ply distribution of $[60°/90°_3/-60°/90°_3/0°/90°_3/0°/90°_3/0°/90°_3/0°_{20}]_S$ is close to the target. The resulting Campbell diagram of the layup A is shown in Fig. 9. The margin to the 1st EO line is sufficient with 13.75% and 17.91% at take-off and design point, respectively. Rotational speeds prone to forced response by the inlet distortions are 6675 RPM with the the 1st mode crossing the 2nd EO, 7485 RPM with the 2nd mode crossing the 5th EO, and at 8640 RPM with the 3rd mode crossing the 6th EO. The resulting logarithmic decrement of the 1st mode of layup A at key operating points for each nodal diameter is shown in Fig. 10. All NDs at take-off and at the design point are stable, with a minimal margin of 4.5 % for ND 1 at take-off condition. The operating point at 8250 RPM and 52.8 kg/s is unstable for the 1st and 2nd ND with a logarithmic decrement of -1.2 % and -0.9 %, respectively.

Figure 11 shows the performance map of the current fan design including stable and unstable operating points regarding the rotor-only flutter and the 1st mode of the composite blade layup A. The unstable NDs of the 1st mode are written next to the unstable operating points. Additionally, the working lines (WLs) for cruise and take-off are shown, which differ because in rig operation the same ambient conditions exist for cruise and take-off. The point at which the CFD last converged is treated as the surge limit of the fan stage for a preliminary estimate. The design is also checked for a sufficient stall margin (SM), with the following target:

$$SM = 1 - \frac{\pi_{t,DP}}{\pi_{t,SL}} \frac{\dot{m}_{SL}}{\dot{m}_{DP}} > 11\% \tag{5}$$

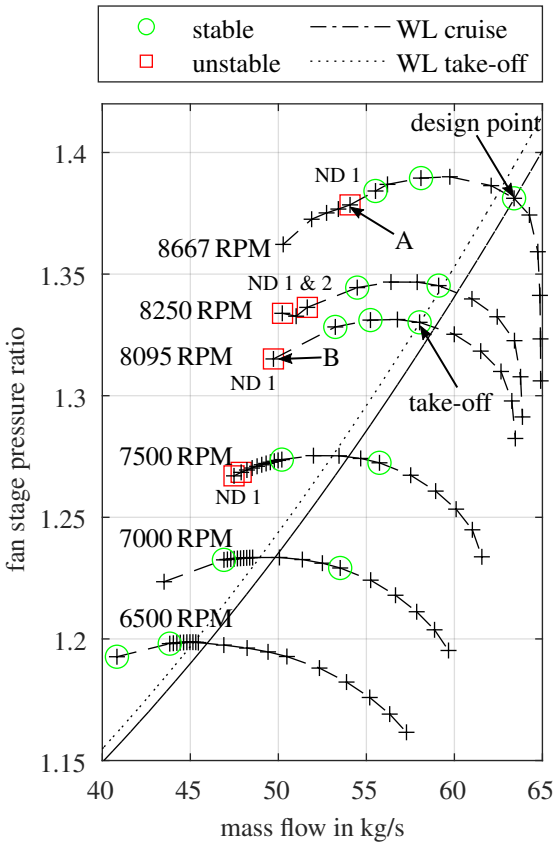

FIGURE 11. FAN PERFORMANCE MAP WITH UNSTABLE OPERATING POINTS

With a stall margin of 19.6% for cruise speed and 16.7% for take-off speed the defined minimum margin of 11% is exceeded. For a finer-resolved surge line, transient simulations must be performed. An operating point is considered unstable if the aerodynamic damping of at least one nodal diameter is negative. Flutter is found at reduced mass flow rates and rotational speeds of 7500 RPM to 8667 RPM close to stall. The fan's radial distribution of total pressure ratio and diffusion factor at cruise and take-off speed are depicted in Fig. 12, showing the tip loading of the fan. This leads to a fan-driven stall, mainly due to separation near the blade tip, which enhances flutter. Although the fan was designed rather conservatively with low values for the diffusion factor, these values increase for partial load at the unstable points A and B, depicted in Fig. 11.

Based on analytical prediction, the rotor can be further stabilized or destabilized at specific rotational speeds by using different intake length. The flutter-simulations of the coupled domain of intake and rotor are still ongoing.

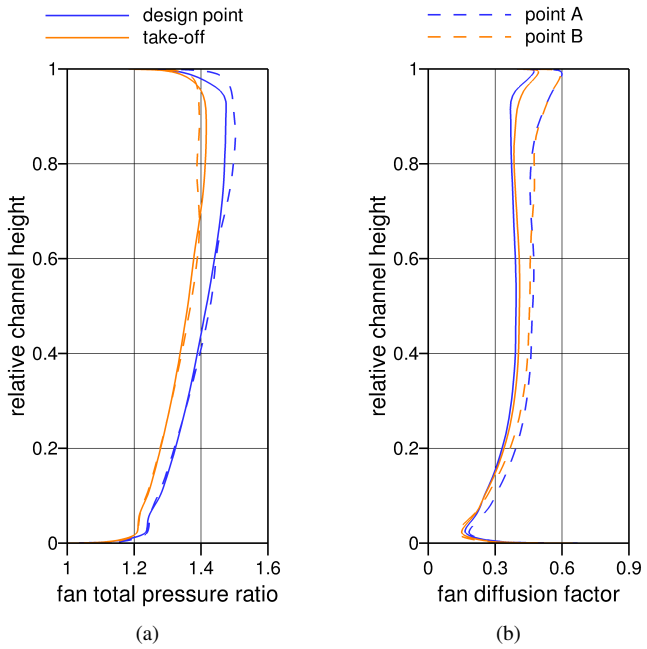

FIGURE 12. RADIAL DISTRIBUTION OF TOTAL PRESSURE RATIO AND DIFFUSION FACTOR OF THE ROTOR

CONCLUSIONS

The CA3ViAR consortium designs and will test a low-speed fan, which develops instability mechanisms representative of UHBR fans of civil aircraft. The aerodynamics, aeroelasticity and aeroacoustics are investigated numerically and experimentally, focusing on extensive flutter measurements. In this paper, the test facility and the instrumentation, as well as the design process of the fan stage, are presented. Based on an engine model for a geared turbofan with a bypass ratio of 17, a fan stage configuration was designed. The preliminary design fulfills all aerodynamic design specifications and achieves a peak polytropic efficiency of 89%. With a surge margin of 19.6%, safe operation can be achieved. The resulting Campbell diagram defines operating points prone to forced response. A target for the structural design of the blade has been identified by performing flutter simulations with varying the eigenfrequency and the mode shape. In a subsequent step, the design process iterates between the flutter simulation and the mechanical design of the composite blade, by analyzing different materials and layups, with the aim to create flutter conditions in some desired operating points by keeping a sufficient margin with respect to the working line. The influence on the aerodynamic damping of the acoustic reflection induced by the intake is modeled analytically, giving an indication whether the blade is stabilized or destabilized by the reflected wave for a specific intake length. Flutter simulation of the coupled intake and rotor are ongoing to complete the aeroelastic design.

The resources of ZENODO are used to disseminate project data and results as open access research, with a link provided on the project website. The types of data and license agreements are specified in the publicly available data management report of the project. First data are expected to be available by the end of 2021, with the full data-set available by the end of the project (2023).

ACKNOWLEDGMENTS

This project has received funding from the Clean Sky 2 Joint Undertaking (JU) under grant agreement No 864256.
The JU receives support from the European Union's Horizon 2020 research and innovation programme and the Clean Sky 2 JU members other than the Union. This is gratefully acknowledge by the authors. Furthermore, the authors would like to acknowledge the German Aerospace Center (Deutsches Zentrum für Luft- und Raumfahrt, DLR) for providing TRACE.

DISCLAIMER

The present work reflects only the authors' view and the European Commission and Clean Sky 2 JU are not responsible for any use that may be made of the information contained in this paper.

REFERENCES

[1] Vahdati, M., Sayma, A. I., Marshall, J. G., and Imregun, M., 2001. "Mechanisms and prediction methods for fan blade stall flutter". *Journal of Propulsion and Power,* ***17***(5), pp. 1100–1108.

[2] Vahdati, M., Simpson, G., and Imregun, M., 2011. "Mechanisms for wide-chord fan blade flutter". *Journal of Turbomachinery,* ***133***(4), p. 54.

[3] Vahdati, M., Lee, K.-B., and Sureshkumar, P., 2020. "A review of computational aeroelasticity of civil fan blades". *International Journal of Gas Turbine, Propulsion and Power Systems,* ***11***(4), pp. 22–35.

[4] Vahdati, M., Smith, N., and Zhao, F., 2015. "Influence of intake on fan blade flutter". *Journal of Turbomachinery,* ***137***(8), p. 54.

[5] Lee, K.-B., Wilson, M., and Vahdati, M., 2016. "Numerical study on aeroelastic instability for a low speed fan". In ASME Turbo Expo 2016, ASME.

[6] Day, I. J., 2016. "Stall, surge, and 75 years of research". *Journal of Turbomachinery,* ***138***(1).

[7] Stapelfeldt, S., and Vahdati, M., 2018. "On the importance of engine-representative models for fan flutter predictions". *Journal of Turbomachinery,* ***140***(8).

[8] Brandstetter, C., Pages, V., Duquesne, P., Paoletti, B., Aubert, S., and Ottavy, X., 2019. "Project phare-2—a high-speed uhbr fan test facility for a new open-test case". *Journal of Turbomachinery,* ***141***(10).

[9] Keen, J. M. S., 1967. "The use of composite materials in aero engines". In SAE Technical Paper Series, SAE Technical Paper Series, SAE International400 Commonwealth Drive, Warrendale, PA, United States.

[10] Kirk, G. E., 1989. "Composite materials for future aero-engines". In ASME 1989 International Gas Turbine and Aeroengine Congress and Exposition, ASME.

[11] Chamis, C. C., 1977. "Vibration characteristics of composite pan blades and comparison with measured data". *Journal of Aircraft,* ***14***(7), pp. 644–647.

[12] Coroneos, R. M., and Gorla, R. S. R., 2012. "Structural analysis and optimization of a composite fan blade for future aircraft engine". *Int. J. Turbo Jet-Engines,* ***29***(3).

[13] Krone, J.-H., and Friedrichs, J., 2015. "Generation of intake distortion due to angle of attack for a high bypass turbofan model". In Proceedings of the ASME International Mechanical Engineering Congress and Exposition - 2014, ASME.

[14] Kurzke, J., 2012. Gasturb: Design and off-design performance of gas turbines.

[15] Grieb, H., 2009. *Verdichter für Turbo-Flugtriebwerke*. Springer Berlin Heidelberg, Berlin, Heidelberg.

[16] Kaplan, B., 2010. *Design of an Advanced Fan Stage With Ultra High Bypass Ratio and Comparison with Experimental Results*. DLR.

[17] Giesecke, D., Lehmler, M., Friedrichs, J., Blinstrub, J., Bertsch, L., and Heinze, W., 2018. "Evaluation of ultra-high bypass ratio engines for an over-wing aircraft configuration". *Journal of the Global Power and Propulsion Society,* ***2***, p. 8SHP7K.

[18] A. Johnsen, Robert o. Bullock. "Aerodynamic design of axial-flow compressors". In *NASA Technical Reports, Special Publication*.

[19] Lieblein, S., 1965. "Experimental flow in two-dimensional cascades". In *NASA SP-36*.

[20] Schlichting, H., and Truckenbrodt, E., 2001. *Aerodynamik des Flugzeuges: Erster Band: Grundlagen aus der Strömungstechnik Aerodynamik des Tragflügels (Teil I)*, 3. auflage ed. Klassiker der Technik. Springer, Berlin and Heidelberg.

[21] Wennerstrom, A. J., 2000. *Design of highly loaded axial-flow fans and compressors*. Concepts ETI, White River Junction, Vt.

[22] Abbott, I. H., and von Doenhoff, A. E., 2012. *Theory of Wing Sections: Including a Summary of Airfoil Data*. Dover Books on Aeronautical Engineering. Dover Publications, Newburyport.

[23] Breard, C., Vahdati, M., Sayma, A. I., and Imregun, M., 2002. "An integrated time-domain aeroelasticity model for the prediction of fan forced response due to inlet distor-

tion". *Journal of Engineering for Gas Turbines and Power,* ***124***(1), pp. 196–208.
[24] Zhao, F., Smith, N., and Vahdati, M., 2017. "A simple model for identifying the flutter bite of fan blades". *Journal of Turbomachinery,* ***139***(7), p. 041029.
[25] Celik, I. B., Ghia, U., Roache, P. J., Freitas, C. J., Coleman, H., and Raad, P. E., 2008. "Procedure for estimation and reporting of uncertainty due to discretization in cfd applications". *Journal of Fluids Engineering,* ***130***(7), p. 078001.
[26] Kato, M., and Launder, B., 1993. "The modelling of turbulent flow around stationary and vibrating square cylinders".
[27] Bardina, J., Ferziger, J. H., and Rogallo, R. S., 1985. "Effect of rotation on isotropic turbulence: computation and modelling". *Journal of Fluid Mechanics,* ***154***, pp. 321–336.
[28] Röber, T., Kožulović, D., Kügeler, E., and Nürnberger, D., 2006. "Appropriate turbulence modelling for turbomachinery flows using a two-equation turbulence model". In New Results in Numerical and Experimental Fluid Mechanics V, H.-J. Rath, C. Holze, H.-J. Heinemann, R. Henke, and H. Hönlinger, eds., Springer Berlin Heidelberg, pp. 446–454.
[29] Langtry, R. B., and Menter, F. R., 2009. "Correlation-based transition modeling for unstructured parallelized computational fluid dynamics codes". *AIAA Journal,* ***47***(12), pp. 2894–2906.
[30] Billman, L. C., 1988. *Large scale prop-fan structural design study. Volume I, Initial concepts*. Hamilton Standard Division, United Technologies [Windsor Locks, Conn.].
[31] Frey, C., Ashcroft, G., Kersken, H.-P., and Voigt, C., 2014. "A harmonic balance technique for multistage turbomachinery applications". In Proceedings of the ASME Turbo Expo: Turbine Technical Conference and Exposition - 2014, H. Hodson, ed., ASME.
[32] Kersken, H.-P., Frey, C., Voigt, C., and Ashcroft, G., 2012. "Time-linearized and time-accurate 3d rans methods for aeroelastic analysis in turbomachinery". *Journal of Turbomachinery,* ***134***(5).

Appendix A: BLADE DESIGN FORMULA

The advanced parabolic mean arc line is expressed in a dimensionless way as:

$$y_c = \frac{b}{x_b}\frac{x_c(1-x_c)}{c\,1+\frac{1-2x_c}{x_b}x_c} \tag{6}$$

The cubic thickness distributions definition depends on the maximum thickness position x_t and consists of a two terms, one upstream of x_t and one downstream of x_t. Here the definition for $x_t \geq 0.5$ is shown.

$$y_1 = a\,x^3 + b\,x^2 + c\,x + d \tag{7}$$

$$y_2 = e(x-x_t)^3 + f(x-x_t)^2 + g(x-x_t) + h \tag{8}$$

The coefficients a to h are given as follows:

$$a = \frac{\frac{t_1}{2}-\frac{t}{2}}{(1-x_t)^3} \qquad e = \frac{\frac{t_2}{2}-\frac{t}{2}}{(1-x_t)^3} - \frac{3}{2x_t^2} + \frac{\frac{t_1}{2}-\frac{t}{2}}{(1-x_t)}$$
$$b = 0 \qquad f = \frac{3}{2x_t^2}\left(\frac{t_1}{2}-\frac{t}{2}\right)$$
$$c = \frac{-3}{2x_t\,\frac{t_1}{2}-\frac{t}{2}} \qquad g = 0$$
$$d = \frac{t_1}{2} \qquad h = \frac{t}{2}$$

The imposition of the thickness distribution on the camberline is defined for suction side and pressure side separately.

$$x_{SS} = x_c - y_c \cdot \sin\theta \qquad y_{SS} = y_c + y_t \cdot \cos\theta \tag{9}$$
$$x_{PS} = x_c + y_c \cdot \sin\theta \qquad y_{PS} = y_c - y_t \cdot \cos\theta \tag{10}$$

Thereby, the local camberline slope is described by the angle θ.